Changes in the TRMM Version-5 and Version-6 Precipitation Radar Products due to Orbit Boost

Liang Liao
Goddard Earth Sciences & Technology Center/UMBC, Greenbelt, MD 20771

and

Robert Meneghini
Code 613.1, NASA/GSFC, Greenbelt, MD 20771

Submitted to
Journal of Meteorological Society of Japan
for Special issue on Satellite Precipitation Observation

Corresponding author information:

Dr. Liang Liao
Goddard Earth Science Technology/UMBC
Code 613.1
NASA/Goddard Space Flight Center
Greenbelt, MD 20771

301-614-5718 (phone)
301-614-5558 (fax)
Email: Liang.Liao-1@ nasa.gov

Abstract

The performance of the version-5 and version-6 Tropical Rainfall Measuring Mission (TRMM) Precipitation Radar (PR) products before and after the satellite orbit boost is assessed through a series of comparisons with Weather Surveillance Radar (WSR)-88D ground-based radar in Melbourne, Florida. Analysis of the comparisons of radar reflectivity near the storm top from the ground radar and both versions of the PR indicates that the PR bias relative to the WSR radar at Melbourne is on the order of 1dB for both pre- and post-boost periods, indicating that the PR products maintain accurate calibration after the orbit boost. Comparisons with the WSR-88D near-surface reflectivity factors indicate that both versions of the PR products accurately correct for attenuation in stratiform rain. However, in convective rain, both versions exhibit negative biases in the near-surface radar reflectivity with version-6 products having larger negative biases than version-5. Rain rate comparisons between the ground and space radars show similar characteristics.

1. Introduction

The Tropical Rainfall Measuring Mission (TRMM) satellite was launched into a low-Earth, low-inclination (35^0) orbit in November 1997. The Precipitation Radar (PR) aboard the TRMM satellite is the first active microwave instrument for measuring three-dimensional storm structures from space (Simpson et al., 1996; Kummerow et al., 2000; Kozu et al., 2001). TRMM rain products, covering the Tropics and subtropics, have been widely used in climate, hydrological cycle and global circulation studies. In August 2001, after nearly four years of successful operations, the TRMM satellite was boosted from an orbital altitude of 350km to 402.5km. This was done to conserve fuel and thus prolong the life of the satellite, which has served to advance our understanding of critical issues related to climate change and global warming. However, the boost of the satellite potentially affects the TRMM measurements and the performance of its rain rate algorithms (Demoss and Bowman, 2007; Cho and Chun, 2008). For example, the boost in altitude increases the TRMM PR near-nadir field of view from 4.3km to 5.0km, and broadens the PR swath width from 215km to 247km (Kozu et al., 2001). As a result, the radar beam-filling problem becomes a more serious issue for the PR algorithms. In addition, a reduction of the PR sensitivity by 1.2dB because of the increased range degrades the capability of the instrument to detect light rain rates. Operating at a frequency of 13.8GHz (Ku band), the PR is subject to attenuation from cloud water, rain and partially melted hydrometeors. A hybrid scheme (Iguchi et al., 2000) is applied to the TRMM PR data to estimate rain attenuation. This is a combination of the surface reference technique (SRT; Meneghini et al., 2000) and the Hitschfeld-Bordan method (1954). In addition to the attenuation correction, accurate radar calibration is essential for reliable estimates of rainfall rate. Although calibration can be performed in a number of ways, the most important external calibration may be

comparisons of the PR-derived radar reflectivities with estimates of the same quantities made with well-calibrated, ground-based radar (Anagnostou et al., 2001; Schumacher and Houze, 2000; Bolen and Chandrasekar, 2000; Liao et al., 2001). The PR calibration can be checked by statistical comparisons between the PR and the unattenuated ground-based radar returns at the top of stratiform storms where dry snow is nearly always the only scattering component present so that attenuation is negligible in the Ku band. The PR attenuation algorithms can be evaluated if similar comparisons are made near the surface.

One of the primary goals of this study is to assess the effects of the orbit boost on the PR calibration and attenuation-correction algorithms as well as on the rain-rate estimates. To this end, we compare the PR data to unattenuated, well-calibrated ground radar measurements that are unaffected by the satellite orbit boost. As a result of the different viewing geometries from space and ground and also because of the different coordinate systems adopted for the data sets, one challenge in comparing satellite data against ground measurements is to merge and co-locate the data onto a common grid. Liao and Meneghini (2009) have recently developed a technique that is designed to transform the data taken from multiple sensors on different platforms to a fixed coordinate system. Using this technique, data can be compared on a pixel level.

In conjunction with analyzing the boost effect, we also compare the PR version-5 and version-6 level-2 products against the ground-radar data. Checking the changes in the PR-updated products with previous results is beneficial not only to understand the physical processes involved but also to provide insight into improving the accuracy of the algorithms (Shige et al., 2006). Moreover, using the subsets of the pre- and post- orbit boost data enables us to look into the issues as to how and to what extent the orbit boost affects the performances of the PR version 5 and 6 algorithms. The PR 2A25 algorithm, which corrects for rain attenuation and estimates

the instantaneous three-dimensional distribution of rain, underwent several major modifications in going from version 5 to version 6. These include: 1) Consideration of attenuation caused by cloud liquid water, water vapor, and molecular oxygen in the attenuation correction algorithm; 2) Estimation of rain attenuation between the lowest range bin that is free from the mainlobe surface clutter and the actual surface by assuming a given slope of the radar reflectivity; 3) Estimation of radar reflectivity, rain and several parameters that vary with the adjustment parameter (ε) of α as the expected values with respect to the posterior probability distribution function of ε; and 4) Re-evaluation of the error estimates in the path-integrated attenuation by the surface-reference technique. A more detailed description of the changes in the PR 2A25 algorithms from version 5 to version 6 can be found at the website: http://tsdis.gsfc.nasa.gov.

The paper is organized as follows. Section 2 gives a brief explanation of the method to match the space and ground data along with a description of the science data used in this study. Comparisons of the radar-reflectivity factors between the PR and ground-based radar are discussed in Section 3 followed by the comparisons of rainfall rates in Section 4. Section 5 provides a summary of the work.

2. Data and Matching Method

2.1 Data

TRMM science data are provided by the TRMM Science Data and Information System (TSDIS) (http://tsdis.gsfc.nasa.gov/tsdis/tsdis.html) and are publicly available from the Goddard Distributed Active Archive Center (GES DISC DAAC) (http://daac.gsfc.nasa.gov/data/datapool/TRMM/index.html). The TRMM version-5 products are available only through February 2004. For this reason, the data used in this study are taken over

the period from January of 1998 to February of 2004. PR products 1C21, 2A23 and 2A25, which provide the respective measured (or apparent) radar reflectivity, storm type classification, and corrected radar reflectivity and estimated rain rate, are used. The ground-based radar measurements are taken from the S-band WSR-88D radar for the same period for the overpasses of the TRMM satellite over the Melbourne, Florida site during times when significant precipitation was present in the overlap region of the PR and WSR-88D. The data are provided by the TRMM Ground Validation (GV) program that has been responsible for processing ground-based measurements from the primary GV sites (Kwajalein Atoll, Republic of the Marshall Islands; Melbourne, Florida; Houston, Texas; and Darwin, Australia), which consist primarily of an operational weather radar and a rain gauge network (Wolff et al., 2005; Houze et al., 2004). The latest version (version 5) of TRMM GV standard products 2A55 and 2A53 is used in the study. GV product 2A55 provides three-dimensional gridded data of the radar reflectivity for WSR-88D with a spatial resolution of 2km × 2km ×1.5km in the x, y (horizontal) and z (vertical) directions over a maximum range of 150km (relative to radar) while GV 2A53 provides two-dimensional surface rain with a horizontal resolution of 2km × 2km. In the present study, 78 TRMM overpasses of Melbourne are obtained before the orbit boost from January 1998 to August 2001 and 63 overpasses are obtained after the boost from September 2001 to February 2004. It should be noted that WSR-88D typically takes approximately six minutes to complete a volume scan while the TRMM satellite overflies the GV site on the order of seconds. The temporal offsets between the PR and WSR for the pixels should be six minutes or less and around three minutes on average.

2.2 Matching Method

One of the challenges in comparing space- and ground-radar data is to map the data onto a common coordinate system. The TRMM PR data are given as functions of latitude, longitude and height in the Earth coordinate system, while WSR-88D ground-radar data are provided in a Cartesian coordinate system in which the x-axis is directed east, the y-axis north, and the z-axis perpendicular to the local surface. Therefore, one of the crucial issues for validating the TRMM PR products using ground-based radar measurements is to register the data in a common coordinate system. This can be done by transforming from one coordinate system to the other. In this study, we will map satellite data onto the local Cartesian coordinates.

During the TRMM pre-boost phase (before August 2001), the TRMM PR near-nadir field of view had a horizontal (vertical) resolution of 4.3km (0.25km) (Kozu et al., 2001). After the boost that raised the orbital altitude from 350km to 402.5km, the horizontal resolution increased to nearly 5km. The resolution volume of the WSR-88D ground-based radar depends strongly on range but the data are typically interpolated to a 1.5km resolution along the vertical and a 2km resolution in the horizontal (Wolff et al., 2005). Considering the data resolutions of both PR and WSR-88D, a common grid element of $4\times4\times1.5\text{km}^3$ is chosen in this study for the comparisons between the PR and WSR-88D data. The Delaunay triangulation algorithm is used to resample the PR data onto the regular grid. Its computational routine is available from the IDL graphical software package (www.ittvis.com). A detailed description of the technique used for the data registration is provided by Liao and Meneghini (2009).

2.3 Data Error Sources

For the TRMM PR, correcting attenuation caused by rain is essential for obtaining accurate rain profiles. As mentioned earlier, the current PR standard algorithm is based on a hybrid

approach that combines the Hitschfeld-Borden method (1954) and the SRT (Meneghini et al., 2000). The SRT is exclusively used for estimates of path-integrated attenuation (PIA) from the PR down to the surface based on the principle that the differences in the radar-normalized surface cross section between rain and rain-free areas are primarily attributed to path attenuation. Because of the intrinsic variability of surface and the changes in the surface scattering properties between the rain and rain-free areas, the SRT is typically used in moderate to heavy rain in which the path attenuation is often much larger than the natural variability. Variation in the surface conditions contributes to the error in the estimates of the path attenuation. In addition to the estimates of PIA, the effect of the non-uniform beam filling (NUBF) of rainfall is an error source (Takahashi et al., 2006). Even though a procedure to correct this effect was implemented in the version-5 PR algorithm, sometimes the results are unrealistic. The assumed raindrop-size distributions in the PR algorithms also affect the amount of the attenuation correction.

The WSR-88D is subject to the same deficiencies and limitations that all operational radars experience when attempting to estimate rainfall. Many of these limitations have been well documented (Wilson and Brandes, 1979; Hunter, 1996). Radar calibration, rain-rate conversion, and corrections for anomalous propagation and clutter suppression as well as range degradation are among the most serious errors that affect the WSR-88D measurements.

The WSR-88D specifications and scanning strategy are described by Crum et al. (1993). Data products such as 2A55 and 2A53 provided by the TRMM GV program are derived from the WSR-88D products and subjected to additional quality-control procedures. The Quality Control (QC) implemented in the GV program is usually very effective in removing spurious echoes such as clutter associated with insects, birds and chaff, and correcting for the effects of anomalous propagation (Marks et al., 2000). For the GV WSR-88D, constant Z-R relationships are

employed throughout the radar volume scans. These are adjusted monthly according to the probability density function (PDF) of the rain rates measured from the surface rain gauge network using the Window Probability Matching Method (WPMM) (Rosenfeld et al., 1994). To evaluate the WSR-88D rainfall product over the Melbourne site, Wolff et al. (2005) have conducted a validation through dependent, quasi-independent and independent approaches. They found that error statistics from both dependent and independent validation techniques show an agreement between gauge-measured and radar-estimated rainfall to within 8%.

3. Comparing Radar-Reflectivity Factors

The radar-reflectivity factor is closely related to the particle-size distribution and backscattering cross section of the individual hydrometeors. Radar attenuation, a loss of signal strength caused by rain and other hydrometeors, depends strongly on the radar frequency. In general, for a given type of hydrometeor, the attenuation tends to increase as radar frequency increases. The TRMM PR that operates at 13.8GHz (Ku-band) generally suffers from moderate attenuation in light rain, and potentially large attenuation in heavy rain. To accurately infer the rainfall rate, the radar reflectivity needs to be corrected for attenuation before it is converted to rain rate. In contrast, WSR-88D, with an operating frequency of 3GHz (S-band), experiences only a small amount of attenuation. As such, its attenuation does not require correction. Comparing the PR-corrected reflectivity factors to those from the non-attenuated WSR-88D near the surface provides a means to evaluate the PR attenuation algorithm. The PR calibration can be checked by comparing the radar reflectivity between the PR and WSR-88D at the top of stratiform storms because at these levels the attenuation in Ku band can usually be neglected. An operational procedure for the TRMM PR calibration can be found in Kummerow et al. (2000)

and Kozu et al. (2001), while the calibration strategies for WSR-88D have been described by many researchers (Anagnostou and Krajewski, 1998; http://www.roc.noaa.gov/eng/BRFCALIB.htm; http://www.qsl.net/n9zia/pdf/2810000C.pdf).

3.1 Relationship between S and Ku band radar-reflectivity factors

For Rayleigh scattering in which particle sizes are much smaller than the wavelength, the radar-reflectivity factor is simply the sum of the sixth power of the particle diameters and is therefore independent of radar wavelength. In S band, it is sufficiently accurate to assume that all the particles (snow and rain) satisfy the Rayleigh approximation. However, this is not the case for Ku band for which some of the larger particles will fall into the non-Rayleigh scattering region. As a consequence, the radar-reflectivity factors in S and Ku bands are not always the same. The differences between the reflectivities in S and Ku bands depend on the phase of the hydrometeors (liquid, frozen or mixed) and the particle-size distributions. It is necessary to consider both factors when comparing radar reflectivity factors between PR and WSR-88D. What follows is a discussion of the radar-reflectivity factors computed in S and Ku bands for snow and rain.

Although the hydrometeor-size distributions can be conveniently described by the gamma distribution in which there are three independent parameters (Braham, 1990; Gorgucci et al., 2000 and 2002), the Marshall-Palmer raindrop-size distribution (1948) and the Gunn-Marshall snow-size distribution (1958) are perhaps the most popular ones in describing microphysical properties of rain and snow under the condition of atmospheric equilibrium (long-term statistical mean). Figure 1 displays the relationships between S- and Ku- band radar-reflectivity factors for snow (dot-dashed line) and rain (dashed line) as computed from the Marshall-Palmer raindrop-

size distribution and the Gunn-Marshall snow-size distribution. In these calculations, a snowflake is treated as a sphere that approximates the mean of the scattering results from an ensemble of the equi-volume non-spherical particles with random orientations. The bulk snow mass density is assumed to 0.3g/cm^3. The Beard and Chuang (1987) shape-size relationship for raindrops is used to compute the radar reflectivity from rain. The symmetry axes of the raindrops, which are assumed to be oblate spheroids without canting, are aligned along the vertical direction. The PR is assumed to view the rain along nadir while the WSR-88D is assumed to view the rain along the horizontal. As seen in Fig. 1, the differences of the radar-reflectivity factors between S and Ku bands behave differently in snow and rain where the Ku-band reflectivity tends to be larger than the S-band reflectivity in rain and its departure from the one-to-one relation (solid line) gradually increases with increasing reflectivity while this trend reverses in the case of snow. These differences diminish as the radar reflectivity decreases as a result of the dominance of Rayleigh scattering at both wavelengths where the reflectivity is wavelength independent. Using a quadratic regression, the relationships between the S- and Ku-band radar-reflectivity factors (in dBZ) are given by following equations:

$$Z_{Ku} = 0.185074 + 1.01378 Z_S - 0.00189212 Z_S^2, \quad (1)$$

for snow, and

$$Z_{Ku} = -1.50393 + 1.07274 Z_S + 0.000165393 Z_S^2, \quad (2)$$

for rain, where Z_{Ku} and Z_S in decibels are the radar-reflectivity factors in Ku and S bands. To directly compare the PR reflectivity factors to WSR-88D, the WSR-88D measured radar reflectivity, Z_S, is replaced by the WSR-derived Z_{Ku}.

3.2 Evaluation of radar-reflectivity factor for TRMM PR

Because the PR algorithms adopt a hybrid attenuation scheme that uses the surface reference technique, the surface background type and behavior (land, ocean and coast) can impact the accuracy of the algorithms. For this reason, we will evaluate the PR reflectivity with respect to surface type. The ground-based WSR-88D radar located at Melbourne near the Atlantic coast in central Florida has served as one of the principal TRMM GV sites. The surface is almost equally divided into land, ocean and coast within the WSR-88D scan area. As the PR and WSR-88D data are interpolated to a common grid (4km×4km×1.5km), the data can be compared on the pixel level. Figure 2 plots the probability density functions (PDF) of the radar-reflectivity factors as derived from the PR version-6 and WSR-88D products at a height of 1.5km from 63 TRMM overpasses made after the orbit boost. The results are grouped into cases of stratiform (top) and convective (bottom) storms as well as surface type: land (left), ocean (middle) and coast (right). The classification of storm types shown in the plots is based exclusively on the PR observations, which follows the TRMM 2A23 product. In 2A23, each PR range profile is classified into either stratiform, convective or "other" (Awaka et al., 1998; http://tsdis.gsfc.nasa.gov/tsdis/tsdis.html). Information is also given with respect to the accuracy of the classification based in part on the vertical and horizontal structure of the storm and whether these analyses lead to the same classification. Since only a very small portion (less 1%) of the data is classified as "other" in 2A23, the focus of our comparisons is on stratiform and convective. The land, ocean and coast information is obtained from 1C21 and based on the Digital Terrain Elevation Dataset (DTED) Intermittent Dataset (DID) generated by the National Aeronautics and Space Administration Jet Propulsion Laboratory (NASA JPL). The "coast" in 1C21 is defined as the surface that is neither water nor land, i.e., a mix of water and land, which can include inland rivers and lakes. The minimum radar reflectivity is set to 18dBZ (the nominal sensitivity of the PR) for both radars in

order to maintain consistency even though the WSR-88D has much higher sensitivity (better than -15dBZ over the entire scan range). To obtain the PDF, only those pixels for which both PR and WSR-88D exceed the minimum radar reflectivity (18dBZ) are used. This means that the pixels chosen in the computations of PDF for both PR and WSR-88D are identical. For reference, the PR-measured reflectivity (free of surface clutter but uncorrected for attenuation), denoted as PR_m, is also included in Fig. 2. The primary difference between the PDF of "PR_m" and the PDF of "PR" (PR corrected reflectivity) is that the latter has been corrected for attenuation. As expected, only a small correction is made for the PDF of stratiform rain in which the rain is generally light. In contrast, for convective rain, a large attenuation correction is made as indicated by the significant shift of the PDF from "PR_m" (no attenuation correction) to "PR" (attenuation-corrected). The PDF of reflectivity from WSR-88D, denoted by WSR^*, is computed based on the adjusted radar reflectivities from the WSR-88D measurements according to (2). Hereafter, WSR^* is referred to as the WSR-88D adjusted radar reflectivity at the frequency of TRMM PR (Ku band) based on (1) for snow and (2) for rain. Figure 2 reveals that the PDF of the PR-corrected reflectivity tends to agree with that of WSR-88D despite some differences in magnitude in the peaks of their PDFs. The mean values of the radar reflectivities given in the brackets provide information on the biases of the PR results relative to WSR-88D.

Similar procedures are employed across a wide range of data that cover the PR version-5 and version-6 products, including comparisons for different altitudes and rain types and between pre- and post-boost periods. Table 1 (2) summarizes the results of the mean radar-reflectivity factors in dB at a height of 7.5km (1.5km). They are derived from the TRMM PR version 5 (V5) and version 6 (V6) algorithms and the same quantities estimated from the WSR-88D (WSR^*) for stratiform and convective storms, denoted by superscripts S and C, from the TRMM overpasses

of the Melbourne, Florida site before (B) and after (A) the orbit boost. As noted earlier, 78 TRMM overpasses are used in the computations for the pre-boost phase, and 63 overpasses, for the post-boost phase. This is true for the computations of both PR version 5 and 6 products. To better visualize the results provided by Tables 1 and 2, a bar-graph is utilized to illustrate the changes in the mean radar reflectivities. Figure 3 shows biases of the PR-corrected radar reflectivity relative to the WSR-88D for stratiform (top) and convective (bottom) rain at a height of 7.5km, an altitude that can be considered near the storm top, where the hydrometeors are primarily dry snow. Note that the selection of the storm top as high as 7.5km is intended to avoid contributions to the radar signal from the melting layer (or bright band) at far ranges. The results are grouped based on the surface type (land, ocean and coast), pre- and post-boost periods, and PR version-5 and version-6 products. As indicated previously, the PR calibration can be checked from the results of stratiform rain at the storm top. Figure 3 indicates that, for stratiform rain, PR is positively biased by 1.05dB for the PR V5 algorithm and 0.82 dB for the PR V6 algorithm before the boost and positively biased by 1.68dB and 1.40dB after the boost. These results remain approximately the same for convective rain despite an abrupt increase in the coastal background data after the boost. This, however, might simply be caused by a sampling problem. The PR version-6 biases are slightly smaller than those of version 5, but the change is not statistically significant. Moreover, the biases in the PR radar-reflectivity factors exhibit little dependence on the surface background, implying that attenuation at the storm top is so small that the attenuation-correction algorithms have almost no effect on the results.

Similar plots are drawn in Fig. 4 to show the PR biases at a height of 1.5km (near the surface) for evaluation of the PR attenuation. It should be mentioned that to properly estimate the PR reflectivity biases near the surface against the WSR-88D measurements, the offsets found at

the stratiform storm top (the PR calibration relative to WSR-88D) should be taken into account. As such, the mean values of the radar reflectivities at a height of 1.5km are adjusted in computations of the biases in Fig. 4 by subtracting 1.05dB and 0.82dB, which are the mean offsets of the reflectivity over land, ocean and coast at storm top (7.5km) between the PR and WSR-88D for stratiform rain, from the PR version-5 and version-6 results of Table 2 before the boost, and 1.68 dB and 1.40 dB after the boost. As can be seen in Fig. 4, there are some noticeable differences in the PR biases of radar reflectivity between the pre- and post-boost periods. For both stratiform and convective rain, the biases decrease for each surface background type in going from the pre-boost to the post-boost period. There are no significant differences in the results between the PR version-5 and version-6 algorithms for stratiform rain where the PR biases for the PR V5 and V6 data are -0.62dB and -0.58dB for the pre-boost period, and -0.23dB and -0.10dB for the post-boost periods. This implies that good accuracy is achieved in the PR attenuation estimation for stratiform rain. For convective rain, the PR reflectivities are negatively biased to some extent even though an improvement is noticed in going from the pre-boost to the post-boost period. Overall, the biases in the PR version-5 reflectivities are smaller than those in the PR version-6 results. Furthermore, comparisons of the biases indicate that the surface background has a marginal effect on the results. This is true for the both stratiform and convective storms. After averaging the biases over land, ocean and coast surfaces, the mean biases of the radar reflectivity become -1.89dB for PR version-5 data and -2.26dB for PR version-6 data before the orbit boost and -1.19dB and -1.65dB after the boost. This suggests that the PR underestimates the attenuation in convective rain and that the PR version-6 algorithm has larger negative biases than the version-5 algorithm.

4. Comparing Rainfall Rate

The rain rates can be compared using the same set of overpasses and an approach similar to that used for the radar reflectivity. However, because of the different viewing geometries from space and ground and also because of the different techniques in estimating the rain rate from the PR and WSR-88D (Wolff et al., 2005; Iguchi et al., 2000), the comparison of the rain rate is not as straightforward as in the case of radar reflectivity. For the PR, the rain rate data are taken from the near-surface rainfall rate product of TRMM 2A25, which is defined as the lowest point in the clutter-free range profile and usually increases in height with incidence angle. The WSR-88D rainfall rates are provided by the 2A53 product in which the surface rain is derived using 1.5km (3km) Constant Altitude Plan Position Indicator (CAPPI) data for near (far) radar ranges. Figure 5 depicts the PDF of near-surface rain rate as derived from the PR version-6 algorithms and the WSR-88D products from 63 TRMM overpasses over Melbourne, Florida for the post-boost period (2001 to 2004). The results are for stratiform (top) and convective (bottom) storms over land (left), ocean (middle) and coast (right). The mean rain rates are given in the brackets in Fig. 5. For consistency, only the pixels for which the PR- and WSR-derived rain rates exceed 0.5mm h^{-1} (PR threshold) are chosen. It is not difficult to see that there is fairly good agreement in rain rates between the PR and WSR-88D estimates for stratiform rain, as demonstrated by the resemblance of the PDF shapes from the PR and WSR-88D even though the PR is unable to measure light rain because of sensitivity limitations. However, a relatively large discrepancy is found between PR and WSR-88D for convective rain as is evident from the different shapes of the PDFs. In this case, the PR exhibits a narrow rain-rate distribution and underestimates the rain at high rain rates relative to the WSR-88D, which also exhibits a much broader distribution. For convective rain, the mean rain rates estimated from PR and WSR-88D are 11.77mm h^{-1} and

14.86mm h^{-1} over land, 11.05mm h^{-1} and 11.85mm h^{-1} over the ocean, and 12.25mm h^{-1} and 14.62mm h^{-1} over the coast. Thus, the PR relative biases in convective rain with respect to the WSR-88D are -21% over land, -7% over the ocean, and -18% over the coast. Note that the PR relative bias is defined by $(\langle R_{PR}\rangle - \langle R_{WSR}\rangle)/\langle R_{WSR}\rangle$, where $\langle R_{PR}\rangle$ and $\langle R_{WSR}\rangle$ are the PR and WSR-88D mean rain rates.

Table 3 summarizes the mean rainfall rates obtained from the TRMM PR version 5 (V5) and version 6 (V6) data along with the same quantities from the WSR-88D products for stratiform and convective (denoted by superscripts S and C) rain for the TRMM overpasses of the Melbourne, Florida site before (B) and after (A) the orbit boost. A bar-graph in Fig. 6 illustrates the PR relative biases (ordinate) with respect to the WSR-88D, based on the data in Table 3. The biases are sorted into land, ocean and coast surfaces with respect to the PR algorithms, and the results of the stratiform (top) and convective (bottom) storms are provided in Fig. 6. As the results demonstrate, the PR exhibits a small relative bias (less than 10%) for stratiform rain for the PR V5 and V6 algorithms but a negative bias as large as 20% for convective rain. The surface background might impact the biases in Fig. 6, but to a degree that is not significant relative to the uncertainties caused by spatial and temporal offsets between the PR and WSR-88D. The relative biases in the PR version-6 algorithm improve slightly after the boost for convective rain whereas those from the version-5 algorithm degrade after the boost. In general, however, PR V5 is less biased than PR V6.

As shown in Fig. 6, there are significant differences between the PR version-5 and version-6 algorithms for convective rain estimates: version 5 exhibits small positive biases and version 6, large negative biases. Quantifying these differences is of great importance for improving the underlying physics and assumptions of the algorithms in going from one version to another.

Some insight can be gained by considering the PR biases as a function of rain rate. Figure 7 presents the PR biases (top) and normalized biases (middle) as well as the PDF (bottom) of the PR-estimated rain as a function of rain rate from the PR version-5 and version-6 algorithms. The PDF plots are included to provide information on the rain-intensity distribution that can be used to identify the statistically important range of rainfall rates. The PR bias at rain rate R, denoted by $\delta(R)$, gives the difference of the mean rain rates between PR and WSR-88D within the interval of (R-ΔR/2, R+ΔR/2):

$$\delta(R) = \frac{1}{N_R}\sum_{n=1}^{N_R}\left(R_{PR}(n) - R_{WSR}(n)\right), \tag{3}$$

where N_R is the total number of pixels in the interval and $R_{PR}(n)$ and $R_{WSR}(n)$ are the PR and WSR-88D rain rates at the nth pixel that satisfy

$$\left|R_{PR} - R\right| \le \frac{\Delta R}{2}, \quad R_{PR} \ge R_{\min} \text{ and } R_{WSR} \ge R_{\min}. \tag{4}$$

In light of (4), the summation in (3) is carried out only over the pixels in which the rain rate exceeds a predefined threshold, R_{min}, from both PR and WSR-88D in addition to the constraint that the PR rain is confined to the interval (R-ΔR/2, R+ΔR/2). ΔR is the bin size and is set to 1mm h^{-1} in this study. As noted earlier, R_{min} is chosen as 0.5mm h^{-1} for both radars. The PR normalized bias, $\delta_N(R)$, is then defined by

$$\delta_N(R) = \delta(R)/R, \tag{5}$$

which gives the fractional bias at rain rate R. Based on equations (3) to (5), the biases are computed with a bin size, ΔR, of 1mm h^{-1}. This bin size is used to obtain a sufficient number samples in each bin size to obtain stable results. In computing the statistics, we have merged the data from different surface backgrounds but have retained the pre- and post-boost periods and the

categories of stratiform, convective and all-rain cases. As depicted in Fig. 7, the PR biases and normalized biases are very small in stratiform storms, and the results from the PR version-5 and version-6 products appear very close for rain rates up to 10mm h^{-1}. Relatively large biases are found only in the heavy rain (>10mm h^{-1}). This is in part due to the fact that some convective storms that have a detectable bright band are classified as stratiform rain. Nevertheless, they are not statistically important because, as indicated by the stratiform PDF, only a very small portion of the stratiform pixels have rain rates greater than 10mm h^{-1}. The mean rain rate of the PR version-5 data (version-6 data), given in the brackets, is 3.48mm h^{-1} (3.88mm h^{-1}), reflecting only about a 10% change in mean rain rate from version 5 to version 6. The results change dramatically for convective rain, in which the PR version-5 tends to agree well with the WSR-88D for most rain rates whereas the PR version-6 has negative biases for all rain rates, with the normalized bias varying from -20% to -50%. The mean values for convective rain change by -27% in going from PR version 5 to version 6. For all rain cases, including data from the stratiform, convective and "other" rain as described earlier, the biases from the PR version-6 rain products lie between the results for stratiform and convective cases. In contrast, the results from the PR version-5 data for the same "all-rain" data set compare well with the WSR-88D rain estimates. The change in the mean rain rate from version 5 to version 6 for this all-rain category is about -12%. It is worth noting that, because of changes in 2A23 in going from version 5 to version 6, the rain classification results (stratiform or convective) are not exactly the same in the two versions. Although this is another source of uncertainty in comparing rain rates, it should not be significant.

5. Summary

In this study a check of the PR performance for the periods before and after the TRMM orbit boost is made through a series of comparisons of the PR products to the WSR-88D ground-based radar in Melbourne, Florida. As WSR-88D is unaffected by the orbit boost, it can serve as a reliable reference or "ground truth" to evaluate changes in the PR data before and after the boost. For PR, the version-6 (current operational version) and version-5 products are used, and their biases relative to the ground-based estimates are analyzed. From January 1998 to February 2004, the period when the PR version-5 data are available, there were 78 TRMM overpasses for which significant rain was present prior to the TRMM orbit boost and 63 overpasses after the boost. The PR calibration has been checked in the snow region (near the top of storm) using these data by comparing the PR reflectivities to those measured from the WSR-88D. The PR attenuation algorithm has been evaluated by means of similar comparisons using near-surface data. To account for the differences of the radar reflectivities between the PR and WSR-88D due to their different frequencies, the measured reflectivity from the WSR-88D is converted to that at the PR frequency (Ku band) by regressing the results of the radar reflectivities computed in S and Ku bands with the Gunn-Marshall snow-size distribution and the Marshall-Palmer raindrop-size distribution, both of which represent long-term average results. In this study, the PR-WSR comparisons are conducted by considering a variety of categories that include different rain types (stratiform and convective) and surface background types (land, ocean and coast) that affect the PR performance.

Analysis of the comparisons of the radar reflectivity made at the top of storm from both version-5 and version-6 products indicates that the PR bias relative to the WSR radar at Melbourne is on the order of 1dB. There are no apparent systematic changes in the results between pre-boost and post-boost periods. As expected, there are also no statistically significant

differences in the biases between the PR version-5 and version-6 algorithms because the PR attenuation-correction algorithm is not a factor in determining the radar reflectivity near the storm top. Near the surface where the effects of attenuation are maximum, the PR biases in radar reflectivity for stratiform rain are approximately the same for all the surface backgrounds for the PR version-5 and version-6 products. The bias, when averaged over the surface backgrounds and the two PR version products, is -0.60dB (-0.17dB) for the pre-boost (post-boost) period, after adjusting for the offsets in the radar reflectivity found near the stratiform storm top. An agreement of the radar reflectivity within 1dB between PR and WSR-88D implies good accuracy in the correction of attenuation in stratiform rain. For convective rain, the PR mean biases of version 5 from all surfaces are -1.89dB before the boost and -1.19dB after the boost; these values are -2.26dB pre-boost and -1.65dB post-boost for version 6. This implies a certain amount of underestimation in the PR attenuation for convective rain.

The mean rain rates estimated from the PR version-5 and version-6 products agree fairly well with those derived from WSR-88D for the both pre- and post-boost periods in the stratiform rain with biases relative to WSR-88D of less than 10% for all surfaces. These biases are marginally dependent on the surface but are not statistically significant. In contrast, there are relatively large biases in the estimates of rain from the PR for convective rain. The PR version-5 rain rates are positively biased while the rain rates from version 6 are negatively biased for the two periods. Although there are slight improvements in the rain estimates from PR version 6 after the orbit boost, the biases still remain relatively large: -20% over land, -9% over the ocean and -17% over the coast. The largely negative biases of the rain rates from PR version-6 seem to be related to the underestimates of the PR reflectivity in convective rain. The rain rates estimated from PR version 5, however, behave differently, and their biases tend to increase after the boost. It is

worth noting that climate changes from the pre- to post-boost periods, indicated by a decrease of the mean rain rates in Table 3 for convective storms after the boost, might also affect the results of our comparisons, but to a lesser extent.

A rain-rate-dependent bias has also been investigated for the PR version-5 and version-6 products by using all the data (merging the pre- and post-boost data) to improve the sample size. It is found that the PR version-5 and version-6 rain algorithms perform equally well in inferring the rain rate for stratiform rain as compared with WSR-88D, but the PR version-6 algorithm reveals biases ranging from -20% to -50% for convective rain. In contrast, the PR version-5 algorithm maintains good accuracy across the range of rain rates.

We conclude from this study that the PR version-5 and version-6 products exhibit reasonably stable calibration after undergoing a change in the orbital altitude and that the attenuation-correction procedure for stratiform rain is fairly accurate for both versions and leads to reasonably good estimates of rainfall rate. The largest difference between the two versions occurs in convective rain where version 6 significantly underestimates both radar reflectivity and rain rate. Note that this study is solely based on the comparisons of the TRMM PR to the ground-based WSR-88D in the overlap regions at the Melbourne site. Considering the variability in climate, our findings should not be generalized to other regions. More studies are needed in the future to look into the details of the PR algorithm performance, such as the angle-bin dependence, and the SRT versus Hitschfeld-Borden method. It is anticipated that our results can offer insight that leads to an improvement of PR algorithms and lay a foundation for testing and validating the Global Precipitation Measuring (GPM) Dual-wavelength Precipitation Radar (DPR) algorithms.

ACKNOWLEDGMENTS

We wish to thank David Wolff, David Marks, and the Goddard Space Flight Center TRMM office for providing ground-based WSR data. This work is supported by Dr. R. Kakar of NASA Headquarters under NASA's Precipitation Measurement Mission (PMM) grant NNH06ZDA001N-PMM.

References

Anagnostou, M. S., C. A. Morales, and T. Dinku, 2001: The use of TRMM precipitation radar observations in determining ground radar calibration biases. *J. Appl. Meteor.*, **39**, 2198-2208.

Anagnostou, E., N. and W. F. Krajewski, 1998: Calibration of the WSR-88D precipitation subsystem. *Wea. Forecasting*, **13**, 396-406.

Awaka, J., T. Iguchi, and K. Okamoto, 1998: Early results on rain type classification by the Tropical Rainfall Measuring Mission (TRMM) precipitation radar. *Proc. 8th URSI Commission F Open Symp.*, Aveiro, Portugal, 143-146.

Beard, K. V., and C. Chung, 1987: A new model for the equilibrium shape of raindrops. *J. Atmos. Sci.*, **44**, 1509-1524.

Bolen, S.M. and V. Chandrasekar, 2000: Quantitative cross validation of space-based and ground-based radar observations. *J. Appl. Met*. **39**, 2071-2079.

Braham, R. R., 1990: Snow particle size spectra in lake effect snows. *J. Appl. Meteor.*, **29**, 200-207.

Cho, H-K, and H-Y Chun, 2008: Impacts on the TRMM data due to orbit boost in the spectral domain. *Geophys. Res. Lett.*, **35**, L01403, doi:10.1029/2007GL032320.

Crum, T. D., R. L. Alberty, and D. W. Burgess, 1993: Recording, archiving, and using WSR-88D data. *Bull. Amer. Meteor. Soc*., **74**, 645-653.

Demoss, J. D., and K. P. Bowman, 2007: Changes in TRMM rainfall due to orbit boost estimated from buoy rain gauge data. *J. Oceanic and Atmos. Tech*., **24**, 1598-1607.

Gorgucci, E., G. Scarchilli, V. Chandrasekar and V. Bringi, 2000: Measurement of mean raindrop shape from polarimetric radar observations. *J. Atmos. Sci*., **57**, 3406-3413.

Gorgucci, E., G. Scarchilli, V. Chandrasekar and V. Bringi, 2002: Estimation of raindrop size distribution parameters from polarimetric radar measurements. *J. Atmos. Sci.,* **59**, 2373-2384.

Gunn, K. L. S., and J.S. Marshall, 1958: The distribution with size of aggregate snowflakes. *J. Meteor.*, **15**, 452-461.

Hitschfeld, W., and J. Bordan, 1954: Errors inherent in the radar measurement of rainfall at attenuating wavelengths. *J. Meteor.*, **11**, 58-67.

Houze Jr., R. A., and co-authors, 2004: Uncertainties in oceanic radar rain maps at Kwajalein and implications for satellite validation. *J. Appl. Meteor*., **43**, 1114-1132.

Hunter, S., 1996: WSR-88D radar rainfall estimation: capability, limitation and potential improvements. *NWA Digest*, **20**, 26-36.

Iguchi, T., T. Kozu, R. Meneghini, J. Awaka and K. Okamoto, 2000: Rain-profiling algorithm for the TRMM precipitation radar. *J. Appl. Meteorol*., **39**, 2038-2052.

Kozu, T, and Coauthors, 2001: Development of precipitation radar onboard the Tropical Rainfall Measuring Mission (TRMM) satellite. *IEEE Trans. Geosci. Remote Sens*., **39**, 102-116.

Kummerow, C., and Coauthors, 2000: The status of the Tropical Rainfall Measuring Mission (TRMM) after two years in orbit. *J. Appl. Meteorol.*, **39**, 1965-1982.

Liao, L., R. Meneghini and T. Iguchi, 2001: Comparisons of rain rate and reflectivity factor derived from the TRMM Precipitation Radar and the WSR-88D over the Melbourne, Florida, site. *J. Atmos. Oceanic Technol.*, **18**, 1959-1974.

Liao, L., and R. Meneghini, 2009: Validation of TRMM precipitation radar through comparison of its multi-year measurements to ground-based radar. *J. Appl. Meteorol. Climatol*. (in press).

Marks, D. A., M. S. Kulie, M. Robinson, D. S. Silberstein, D. B. Wolff, B. S. Ferrier, E. Amitai, B. Fisher, J. Wang, D. Augustine, and O. Thiele, 2000: Climatological processing and product development for the TRMM ground validation program. *Phys. Chem. Earth (B)*, **25**, 871-875.

Marshall, J. S., and W.M. Palmer, 1948: The distribution of raindrops with size. *J. Appl. Meteor.*, **5**, 165-166.

Meneghini, R., T. Iguchi, T. Kozu, L. Liao, K. Okamoto, J. A. Jones, and J. Kwiatkowski, 2000: Use of the surface reference technique for path attenuation estimates from TRMM precipitation radar. *J. Appl. Meteor.*, **39**, 2053-2070.

Rosenfeld, D., D. B. Wolff, and E. Amitai, 1994: The window probability matching method for rainfall measurements with radar. *J. Appl. Meteor.*, **33**, 682-693.

Schumacher, C., and R. A. Houze, 2000: Comparison of radar data from the TRMM satellite and Kwajalein ocean validation site. *J. Appl. Meteor*., **39**, 2151-2164.

Shige, S., H. Sasaki, K. Okamoto, and T. Iguchi, 2006: Validation of rainfall estimates from the TRMM precipitation radar and microwave imager using a radiative transfer model: 1. Comparison of the version-5 and -6 products. *Geophys. Res. Lett*., **33**, L13803, doi:10.1029/2006GL026350.

Simpson, J., C. Kummerow, W.-K. Tao, and R. F. Adler, 1996: On the Tropical Rainfall Measuring Mission (TRMM). *Meteor. Atmos. Phys.*, **60**, 19-36.

Takahashi, N., H. Hanado, and T. Iguchi, 2006: Estimation of path-integrated attenuation and its nonuniformity from TRMM/PR range profile data. *IEEE Trans. Geosci. Remote Sens.*, 44, 3276-3283.

Wilson, J. and E. Brandes, 1979: Radar measurement of rainfall: a summary. *Bull. Amer. Meteor. Soc.*, **60**, 1048-1058.

Wolff, D. B., D. A. Marks, E. Amitai, D. S. Silberstein, B. L. Fisher, A. Tokay, J. Wang, and J. L. Pippitt, 2005: Ground validation for the Tropical Rainfall Measuring Mission (TRMM). *J. Atmos. Oceanic Technol.*, **22**, 365-380.

Table 1. Means of radar-reflectivity factors (dBZ) derived from the TRMM PR version 5 (V5) and version 6 (V6) algorithms and the same quantities converted from the WSR-88D measurements (WSR^*) for stratiform (^{S}) and convective (^{C}) storms at a height of 7.5km from TRMM overpasses of Melbourne, Florida before (B) and after (A) the boost of the TRMM satellite orbit.

	Land			Ocean			Coast		
	$\langle PR_m \rangle$	$\langle PR \rangle$	$\langle WSR^* \rangle$	$\langle PR_m \rangle$	$\langle PR \rangle$	$\langle WSR^* \rangle$	$\langle PR_m \rangle$	$\langle PR \rangle$	$\langle WSR^* \rangle$
V5(B)^S	21.72	21.66	20.41	21.08	21.03	20.19	21.69	21.66	20.59
V6(B)^S	21.35	21.34	20.37	20.78	20.77	20.18	21.39	21.41	20.52
V5(A)^S	21.80	21.74	20.01	22.03	21.98	20.25	21.97	21.94	20.36
V6(A)^S	21.42	21.39	19.96	21.75	21.73	20.26	21.62	21.64	20.35
V5(B)^C	26.50	26.49	25.39	25.14	25.17	23.83	26.30	26.47	25.21
V6(B)^C	25.10	25.11	24.31	24.07	24.11	22.92	24.83	24.95	24.12
V5(A)^C	25.58	25.55	24.01	25.09	25.05	23.57	26.46	26.50	24.02
V6(A)^C	24.47	24.44	23.13	23.85	23.82	22.49	25.39	25.36	23.34

Table 2. Means of radar-reflectivity factors (dBZ) derived from TRMM PR version 5 (V5) and version 6 (V6) algorithms and the same quantities converted from WSR-88D measurements (WSR^*) for stratiform (^{S}) and convective (^{C}) storms at the height of 1.5km from TRMM overpasses of Melbourne, Florida before (B) and after (A) the boost of the TRMM satellite orbit.

	Land			Ocean			Coast		
	$<PR_m>$	<PR>	$<WSR^*>$	$<PR_m>$	<PR>	$<WSR^*>$	$<PR_m>$	<PR>	$<WSR^*>$
V5(B)^S	27.29	27.63	26.94	27.57	27.98	27.72	27.02	27.35	27.02
V6(B)^S	26.99	27.56	27.06	27.39	28.02	27.95	26.76	27.29	27.14
V5(A)^S	28.07	28.50	27.02	27.54	27.88	26.66	28.20	28.61	26.97
V6(A)^S	27.83	28.48	27.12	27.33	27.83	26.79	27.91	28.56	27.06
V5(B)^C	32.30	35.69	36.22	32.99	35.86	36.95	31.98	34.72	35.63
V6(B)^C	31.43	33.93	35.11	32.10	34.37	36.03	31.05	33.25	34.73
V5(A)^C	32.59	35.37	35.09	32.42	34.65	34.00	32.92	35.80	35.27
V6(A)^C	31.08	34.01	34.56	31.64	33.42	33.43	32.21	34.51	34.71

Table 3. Means of rain rates (mm h^{-1}) derived from TRMM PR version 5 (V5) and version 6 (V6) algorithms as well as WSR-88D for stratiform (^{S}) and convective (^{C}) storms from TRMM overpasses of Melbourne, Florida before (B) and after (A) the boost of the TRMM satellite orbit.

	Land		**Ocean**		**Coast**	
	$\langle R_{PR} \rangle$	$\langle R_{WSR} \rangle$	$\langle R_{PR} \rangle$	$\langle R_{WSR} \rangle$	$\langle R_{PR} \rangle$	$\langle R_{WSR} \rangle$
V5(B)^{S}	3.51	3.48	3.57	3.79	3.44	3.85
V6(B)^{S}	3.85	3.63	4.19	3.89	3.84	3.98
V5(A)^{S}	3.67	3.66	3.24	3.12	3.50	3.54
V6(A)^{S}	3.91	3.81	3.62	3.30	3.91	3.67
V5(B)^{C}	16.57	16.21	16.38	15.50	16.39	16.23
V6(B)^{C}	12.67	16.93	12.88	16.09	12.45	16.73
V5(A)^{C}	15.41	14.54	13.16	11.43	15.50	14.16
V6(A)^{C}	11.77	14.86	11.05	11.85	12.25	14.62

Figure Captions:

Fig. 1. Relationships between the radar-reflectivity factors in S and Ku bands for snow (dotted-dashed line) and rain (dashed line). In these computations, the Gunn-Marshall (1958) snow-size distribution is assumed with a snow density of 0.3 g/cm^3 for snow; for rain, the Marshall-Palmer raindrop-size distribution (1948) is used. Solid line represents one-to-one relation.

Fig. 2. Probability density functions (PDF) of the radar-reflectivity factors as derived by the PR version 6 algorithm and WSR-88D measurements at a height of 1.5km from 63 TRMM overpasses over Melbourne, Florida after the TRMM orbit boost. "PR_m" ("PR") represents the PR measured (corrected) reflectivities; "WSR^*" refers to the data coming from the WSR-88D but corrected for non-Rayleigh effects at 13.8GHz. The mean values of the radar reflectivities are given in brackets.

Fig. 3. Differences between the mean radar-reflectivity factors for the PR attenuation-corrected (<PR>) and the WSR-estimated (<WSR*>) data at a height of 7.5km for stratiform rain for the PR version 5 (V5) and 6 (V6) results for the TRMM overpasses before (B) and after (A) the boost.

Fig. 4. Differences between the mean radar-reflectivity factors for the PR attenuation-corrected (<PR>) and the WSR-estimated (<WSR*>) results at a height of 1.5km for convective rain for PR version 5 (V5) and 6 (V6) data for overpasses before (B) and after (A) the boost. Note that the mean values of the radar reflectivities are adjusted by subtracting 1.05dB and 0.82dB, which are the mean offsets of the reflectivity over land, ocean and coast at storm top (7.5km) between the PR and WSR-88D for stratiform rain, from the PR version-5 and version-6 results of Table 2 before the boost, and 1.68dB and 1.40dB after the boost.

Fig. 5. Probability density function (PDF) of near-surface rain rate as derived by the PR version-6 algorithms and WSR-88D from 63 TRMM overpasses over Melbourne, Florida after the TRMM orbit boost. "PR" ("WSR^*") represents the PR-derived (WSR-derived) rain rate. The mean values of the rain rates are given in brackets.

Fig.6. Comparisons of relative biases of PR-estimated mean rain rates from version 5 (V5) and 6 (V6) algorithms with respect to WSR-88D estimates before (B) and after (A) the TRMM orbit boost for stratiform (top) and convective (bottom) rain.

Fig. 7. PR rain-rate-dependent biases (top) and normalized biases (middle) as derived from the PR version-5 (solid lines) and version-6 (dashed lines) algorithms relative to the estimates from WSR-88D for stratiform, convective and all-rain cases. The probability density functions (bottom) are also plotted. The mean rain rates are provided in brackets.

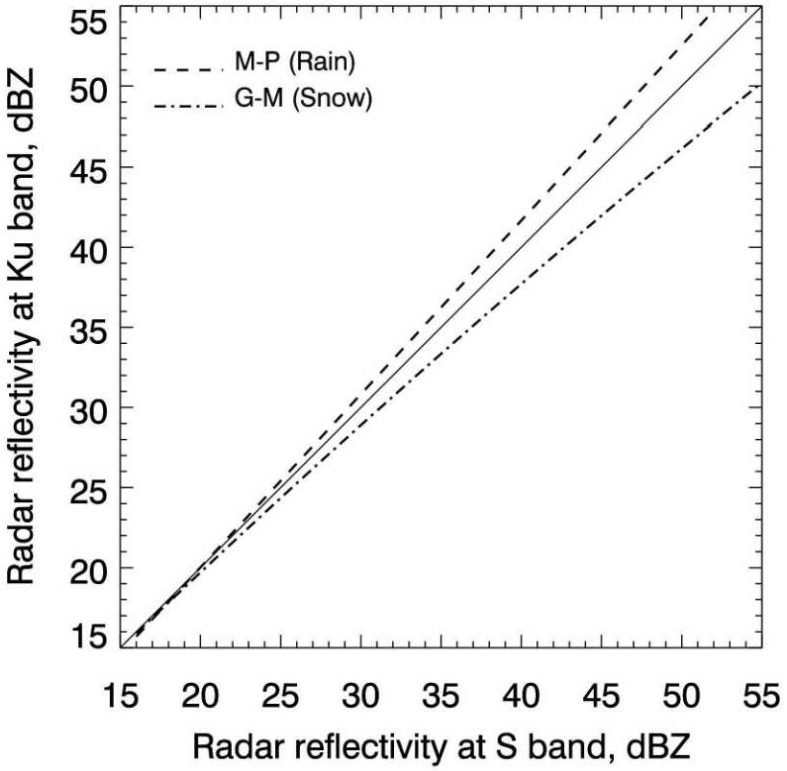

Fig.1 Relationships between the radar reflectivity factors at S and Ku bands for snow (dotted-dashed line) and rain (dashed line). In these computations, the Gunn Marshall (1958) snow size distribution is assumed with a snow density of 0.3 g/cm^3 for snow; and for rain the Marshall-Palmer raindrop size distribution (1948) is used. Solid line represents one-to-one relation.

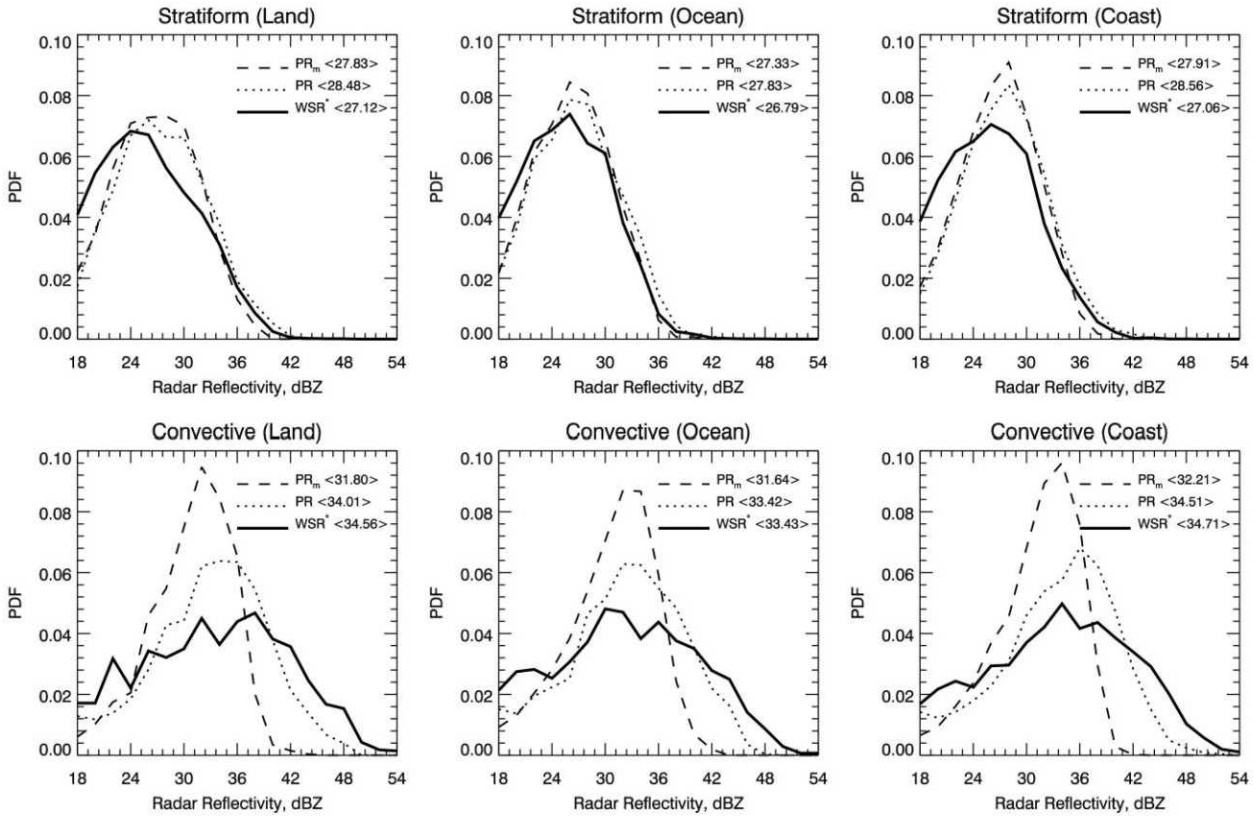

Fig.2 Probability density functions (PDF) of the radar reflectivity factors as derived by the PR version 6 algorithms and the WSR-88D measurements at the height of 1.5 km from 63 TRMM overpasses over Melbourne, Florida after the TRMM orbit boost. "PR_m" and "PR" represent the PR measured and corrected reflectivities, respectively, while "WSR^*" refers to the data coming from the WSR-88D but corrected for non-Rayleigh effects at 13.8 GHz. The mean values of the radar reflectivities are given in the brackets.

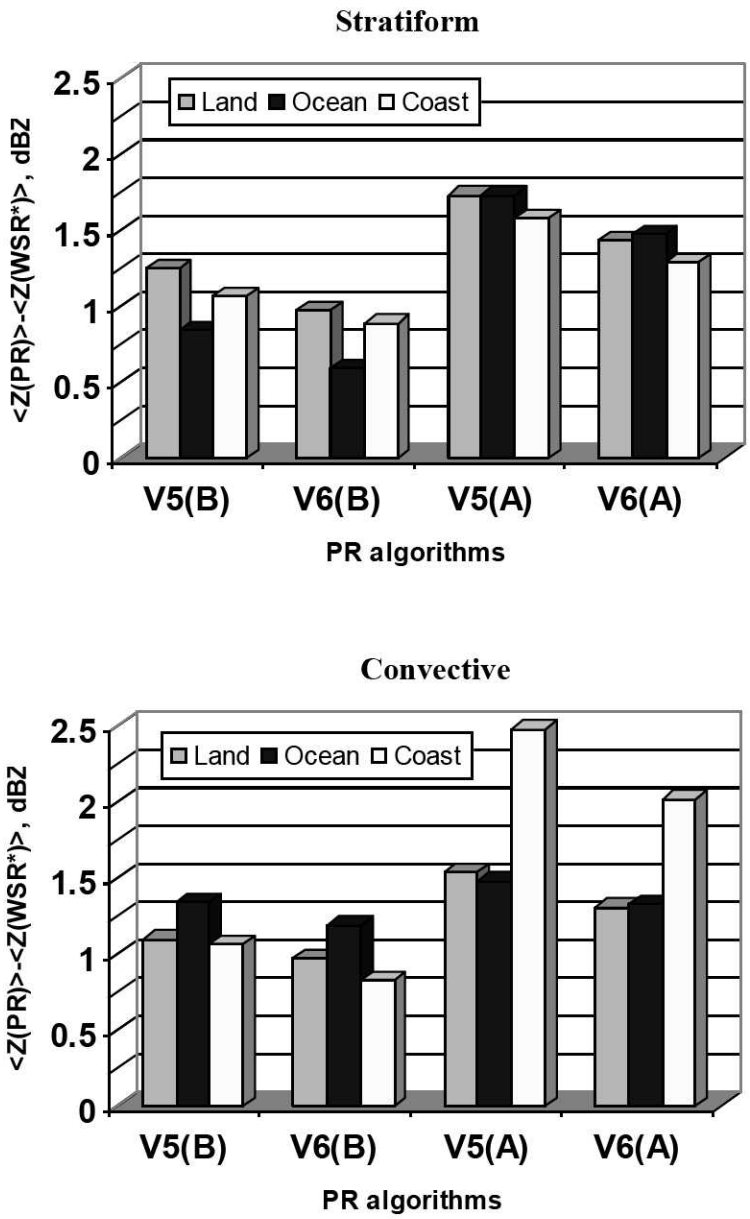

Fig.3 Differencess between the mean radar reflectivity factors for the PR attenuation-corrected (<PR>) and the WSR-estimated (<WSR*>) data at a height of 7.5 km for the case of stratiform rain for the PR version 5 (V5) and 6 (V6) results for the TRMM overpasses before (B) and after (A) the boost.

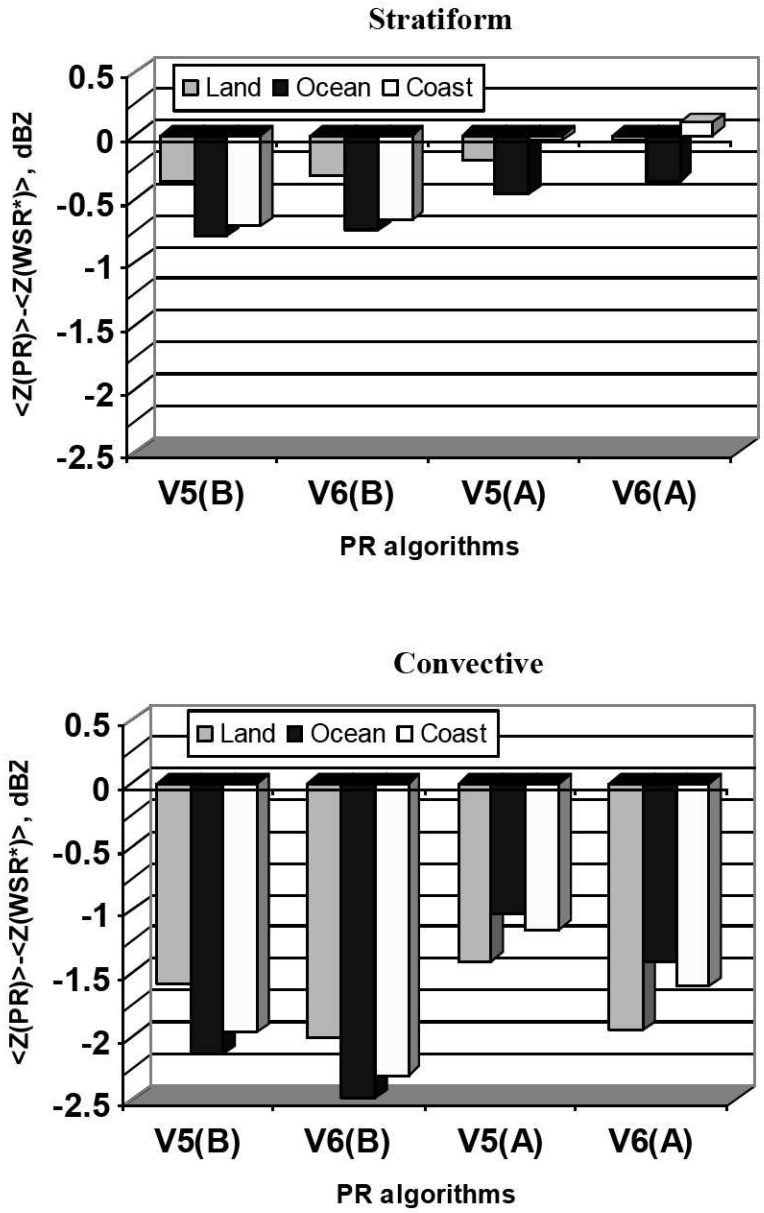

Fig.4 Differences between the mean radar reflectivity factors for the PR attenuation-corrected (<PR>) and the WSR-estimated (<WSR*>) results at a height of 1.5 km for convective rain for PR version 5 (V5) and 6 (V6) data for overpasses before (B) and after (A) the boost. Note that the mean values of the radar reflectivities are adjusted by subtracting 1.05 dB and 0.82 dB, which are the mean offsets of the reflectivity over land, ocean and coast at storm top (7.5 km) between the PR and WSR-88D for stratiform rain, from the PR version-5 and version-6 results of Table 2 before the boost, respectively, and 1.68 dB and 1.40 dB after the boost.

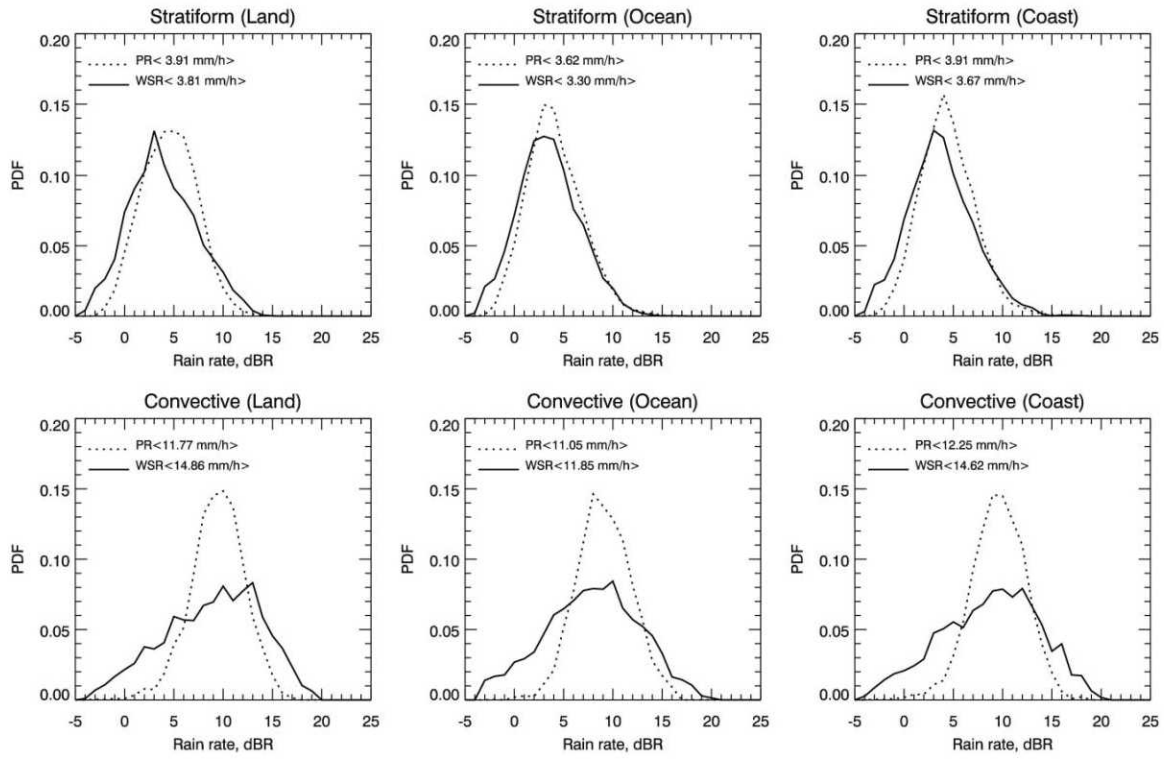

Fig.5 Probability density function (PDF) of near-surface rain rate as derived by the PR version-6 algorithms and the WSR-88D from 63 TRMM overpasses over Melbourne, Florida after the TRMM orbit boost. "PR" and "WSR*" represent the PR- and WSR-derived rain rates, respectively. The mean values of the rain rates are given in the brackets.

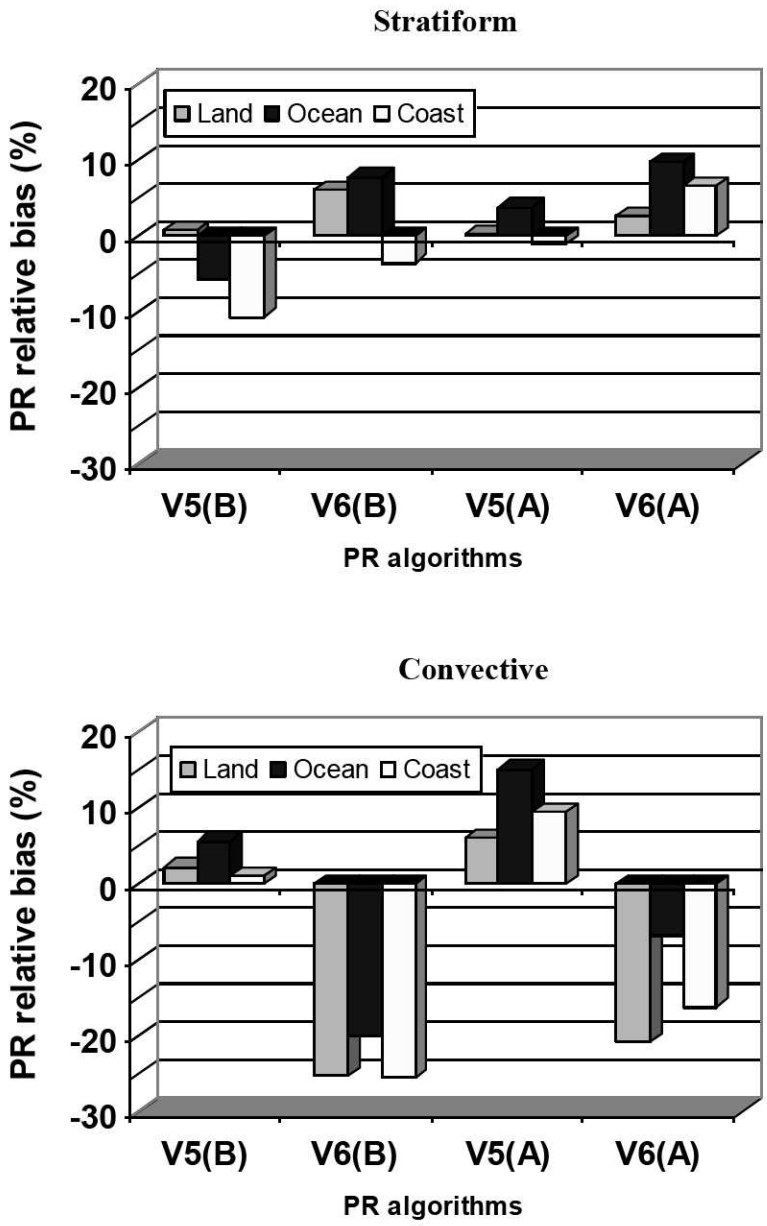

Fig.6 Comparisons of the relative biases of the PR-estimated mean rain rates from versions 5 (V5) and 6 (V6) algorithms with respect to the WSR-88D estimates before (B) and after (A) the TRMM orbit boost for the case of the stratiform (top) and convective (bottom) rain.

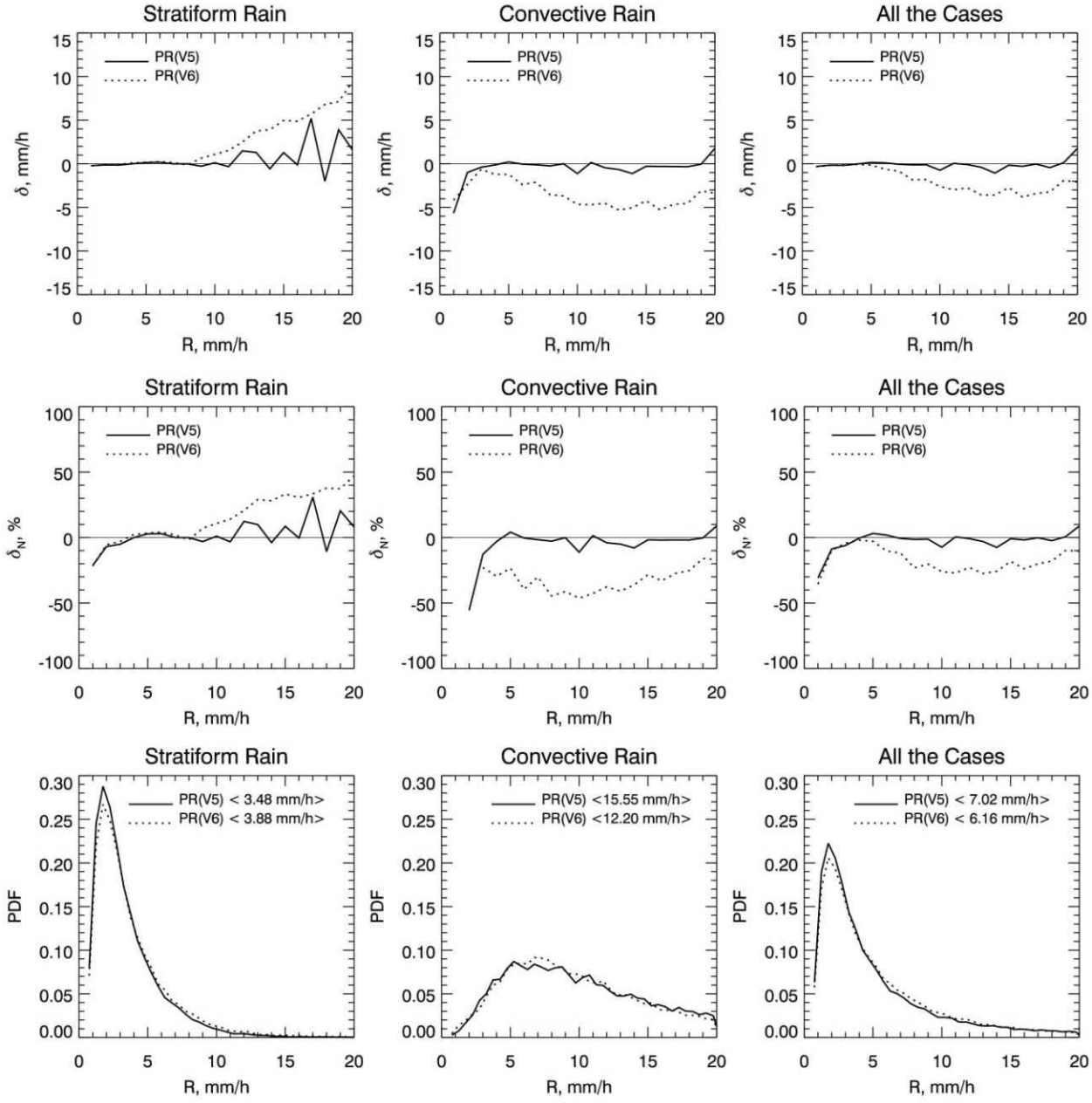

Fig.7 The PR rain-rate-dependent biases (top) and normalized biases (middle) as derived from the PR version-5 (solid lines) and version-6 (dashed lines) algorithms relative to the estimates from the WSR-88D for the stratiform, convective and all-rain cases. The probability density functions (bottom) are also plotted. The mean rain rates are provided in the brackets.

Liao, L., and Robert Meneghini, 2009: Changes in the TRMM version-5 and version-6 precipitation radar products due to orbit boost. *J. Meteor. Soc. Japan*, **87A**, 93-107.

Abstract

The performance of the version-5 and version-6 Tropical Rainfall Measuring Mission (TRMM) Precipitation Radar (PR) products before and after the satellite orbit boost is assessed through a series of comparisons with Weather Surveillance Radar (WSR)-88D ground-based radar in Melbourne, Florida. Analysis of the comparisons of radar reflectivity near the storm top from the ground radar and both versions of the PR indicates that the PR bias relative to the WSR radar at Melbourne is on the order of 1dB for both pre- and post-boost periods, indicating that the PR products maintain accurate calibration after the orbit boost. Comparisons with the WSR-88D near-surface reflectivity factors indicate that both versions of the PR products accurately correct for attenuation in stratiform rain. However, in convective rain, both versions exhibit negative biases in the near-surface radar reflectivity with version-6 products having larger negative biases than version-5. Rain rate comparisons between the ground and space radars show similar characteristics.